Characterization of the Eddy Dissipation Model for the Analysis of Hydrogen-fueled Scramjets

J.J.O.E Hoste[*]**, M. Fossati**

University of Strathclyde
Department of Mechanical and Aerospace Engineering, Aerospace Centre of Excellence
Glasgow
United Kingdom

I.J. Taylor

University of Glasgow
Division of Aerospace Sciences, School of Engineering
Glasgow
United Kingdom

R.J. Gollan

University of Queensland
School of Mechanical and Mining Engineering, Centre for Hypersonics
Brisbane
Australia

[*]
 Currently research fellow at German Aerospace Center, Institute of Aerodynamics and Flow Technology, Göttingen. jimmy-john.hoste@dlr.de

.

2

ABSTRACT

The Eddy Dissipation Model (EDM) is analyzed with respect to the ability to address the turbulence-combustion interaction process inside hydrogen-fueled scramjet engines designed to operate at high Mach numbers ($\approx$ 7-12). The aim is to identify the most appropriate strategy for the use of the model and the calibration of the modeling constants for future design purposes. To this end, three hydrogen-fueled experimental scramjet configurations with different fuel injection approaches are studied numerically. The first case consists of parallel fuel injection and it is shown that relying on estimates of ignition delay from a one-dimensional kinetics program can greatly improve the effectiveness of the EDM. This was achieved through a proposed zonal approach. The second case considers fuel injection behind a strut. Here the EDM predicts two reacting layers along the domain which is in agreement with experimental temperature profiles close to the point of injection but not the case any more at the downstream end of the test section. The first two scramjet test cases demonstrated that the kinetic limit, which can be applied to the EDM, does not improve the predictions in comparison to experimental data. The last case considered a transverse injection of hydrogen and the EDM approach provided overall good agreement with experimental pressure traces except in the vicinity of the injection location. The EDM appears to be a suitable tool for scramjet combustor analysis incorporating different fuel injection mechanisms with hydrogen. More specifically, the considered test cases demonstrate that the model provides reasonable predictions of pressure, velocity, temperature and composition.

NOMENCLATURE

Roman Symbols

s

$\bar{a}$	$= a + a'$, Reynolds average of variable a
$\tilde{a}$	$= a + a''$, Favre average of variable a
a', a''	fluctuating part in decomposition of a
A	Arrhenius pre-exponential constant
A_{edm}	constant number one of the EDM
B_{edm}	constant number two of the EDM
E	mixture total energy per unit mass (J/kg)
H	mixture total enthalpy per unit mass (J/kg)
I	turbulence intensity (%)
J_{s_j}	diffusion flux components of species s ($kg/(m^2 s)$)
k	turbulent kinetic energy (J/kg)
k_f	forward reaction rate constant
k_r	backward reaction rate constant
M	Mach number
$\dot{m}_s$	mass flow rate (kg/s)
Pr_t	turbulent Prandtl number
p	static pressure (Pa)
p_{pitot}	Pitot pressure (Pa)
p_{ref}	Reference total pressure (Pa)
q_j	heat flux components (W/m^2)

Sc_t	turbulent Schmidt number
s	mass stochiometric ratio
T	static temperature (K)
T_A	Arrhenius activation temperature (K)
$T_0 = T_{tot}$	total temperature (K)
T_{ref}	Reference total temperature (K)
t	time (s)
u_i	velocity components (m/s)
W_s	molar mass of species s (kg/mol)
X_s	molar fraction of species s
$[X_s]$	molar concentration of species s (mol/m^3)
x_j	cartesian coordinates (m)
Y_s	mass fraction of species s

Greek Symbols

β^*	= 0.09, turbulence model constant
δ_{ij}	kronecker delta: 0 ($i \neq j$), 1 ($i = j$)
Δy_{reac}	reaction zone thickness
ϵ	dissipation of turbulent kinetic energy (m^2/s^3)
η_c	combustion efficiency
μ_t/μ	ratio of turbulent to laminar viscosity
ν'_m	forward stochiometric coefficient
ν''_m	reverse stochiometric coefficient
ρ	mixture density (kg/m^3)
$\bar{\rho}\widetilde{u''_i u''_j}$	Reynolds stress tensor components ($kg/(ms^2)$)
τ_{ij}	molecular stress tensor components ($kg/(ms^2)$)
ω	dissipation rate of turbulent kinetic energy ($1/s$)
$\dot{\omega}_s$	reaction rate of species s ($kg/(m^3 s)$)

Abbreviations

AUSMDV	Advection Upstream Splitting Method combining Difference and Vector splitting
BLS	boundary layer section
CFD	Computational Fluid Dynamics
DLR	German Aerospace Center
EBU	Eddy Break Up
EDM	Eddy Dissipation Model
EFM	Equilibrium Flux Method
FRC	finite rate chemistry
HEG	High Enthalphy Shock Tunnel Göttingen
LES	Large-Eddy Simulation
MDO	Multi-disciplinary Design Optimization
RANS	Reynolds-Averaged Navier-Stokes
SPARTAN	Scramjet Powered Accelerator for Reusable Technology AdvaNcement
TCI	Turbulence / Chemistry Interaction
URANS	Unsteady Reynolds-Averaged Navier-Stokes

1.0 INTRODUCTION

Scramjet technology has been the subject of many studies since the late 1950s as it provides an efficient means of flying at hypersonic speeds. Potential applications include hypersonic cruise vehicles and access-to-space systems with hydrogen and hydrocarbon as potential fuels. For example, the Australian Scramjet Powered Accelerator for Reusable Technology AdvaNcement (SPARTAN) program aims at exploring the advantages of hydrogen-fueled scramjets by designing a three-stage-to-orbit rocket-scramjet-rocket launch system with reusable first and second stages[1,2]. As an accelerator for access-to-space, the high Mach regime ($\approx$ 7-12) at which a scramjet will operate is characterized by a combustion process which can be considered to be mainly mixing limited[3,4,5]. For design purposes, it is desirable to have a computational technique that can run effectively and efficiently account for turbulence / chemistry interaction (TCI) in the mixing-limited combustion process, and, subsequently, assess the overall combustor performance.

Numerical tools with different levels of fidelity are extensively used in the design of scramjets. Quasi-one-dimensional models have been developed which rely on simplified assumptions to describe the supersonic combustion process[6,7,8]. Being computationally cheap, such low-fidelity approaches are attractive for integration as a subsystem in a complete vehicle analysis as well as in Multi-disciplinary Design Optimization (MDO). However, in some cases these methods may not provide a sufficient level of accuracy or consistency with the physics when complex engine configurations are considered. Steps are being taken towards the improvement of the mixing and combustion models for such low-fidelity methods by introducing surrogates informed by more accurate Computational Fluid Dynamics (CFD) approaches[9] capable of capturing the complex flow field inside scramjets and to account explicitly for the turbulence-chemistry interaction mechanisms inside the combustor section of the engine. Chemically reactive Reynolds-Averaged Navier-Stokes (RANS) still remains the most used approach when targeting design[10,11]. This is mainly related to its more manageable computational cost with respect to methods like LES (Large-Eddy Simulations) or hybrid RANS/LES which can provide superior accuracy and insight into the detailed physics of the combustion mechanism but at a higher computational expense.

In the context of RANS-based approaches, the Eddy Dissipation Model (EDM) introduced by Magnussen and Hjertager[12] is a capable approach to address TCI for mixing-limited scramjets. The use of EDM in the modeling of hydrogen-fueled scramjet flows has been reported in the literature by Edwards et al.[13] using the REACTMB CFD solver and it has also been largely documented in the case of commercially available software[14,15,16,17]. However, little information is found in the open literature about the optimal use of the EDM for scramjets with different types of fuel injection configurations or possible improvements of the model to increase its accuracy. The specification of the model parameters are not always communicated and no consistent guidelines are found regarding their setting. The EDM has as well been reported in the literature for hydrocarbon-fueled scramjets and an overview can be found in[18]. It is however not tackled in the present work and is left for future considerations.

The aim of the present work is to elaborate on the capability of the EDM in addressing supersonic mixing-limited combustion processes inside scramjets which rely on hydrogen

fuel. The optimal use of the model is inferred for three specific scramjet combustors that conceptually represent the most relevant configurations based on different fuel injection schemes: parallel, strut and jet-in-crossflow. This is achieved by analyzing the specification of model constants as well as alternatives to the standard EDM including a kinetic limit and zonal formulation.

The paper is structured as follows. In Section 2, the RANS equations for turbulent reacting flows are presented as well as the detailed formulation of the EDM. Section 3 describes the scramjet test cases used in this work followed by the results of the simulations. A critical discussion summarizing the results is presented in Section 4. Final remarks and proposed future directions are reported in Section 5.

2.0 NUMERICAL MODELING OF SCRAMJETS

The governing equations for turbulent compressible reacting flows can be written as

Mass Conservation:

$$\frac{\partial \bar{\rho}}{\partial t} + \frac{\partial}{\partial x_i}\left(\bar{\rho}\tilde{u}_i\right) = 0 \qquad \ldots(1)$$

Momentum Conservation:

$$\frac{\partial}{\partial t}\left(\bar{\rho}\tilde{u}_i\right) + \frac{\partial}{\partial x_j}\left(\bar{\rho}\tilde{u}_j\tilde{u}_i + \delta_{ij}\bar{p}\right) = \frac{\partial}{\partial x_j}\left(\bar{\tau}_{ji} - \bar{\rho}\widetilde{u_i''u_j''}\right) \qquad \ldots(2)$$

Energy Conservation:

$$\frac{\partial}{\partial t}\left(\bar{\rho}\tilde{E}\right) + \frac{\partial}{\partial x_j}\left(\bar{\rho}\tilde{u}_j\tilde{H}\right) = \frac{\partial}{\partial x_j}\left(\bar{\tau}_{ij}\tilde{u}_i + \overline{\tau_{ij}u_i''} - \bar{q}_j - \bar{\rho}\widetilde{H''u_j''}\right) \qquad \ldots(3)$$

Species Conservation:

$$\frac{\partial(\bar{\rho}\tilde{Y}_s)}{\partial t} + \frac{\partial(\bar{\rho}\tilde{Y}_s\tilde{u}_j)}{\partial x_j} = \bar{\omega}_s - \frac{\partial}{\partial x_j}\left(\bar{J}_{s_j} + \bar{\rho}\widetilde{Y_s''u_j''}\right) \qquad \ldots(4)$$

with conserved variables $\bar{\rho}$, $\bar{\rho}\tilde{u}_j$, $\bar{\rho}\tilde{E}$, $\bar{\rho}\tilde{Y}_s$ representing density, momentum, total energy per unit volume and partial densities of the species s (s=1,...,N). Throughout this work, the above set of equations will be referred to as the Reynolds Averaged Navier-Stokes equations (RANS). The symbols $\bar{x}$ and $\tilde{x}$ denote respectively the time and Favre (or density-weighted) average. Equations (1) to (4) are written in such a way that those terms which require modeling are indicated on the right-hand side. The system of conservation equations for a turbulent chemically reacting flow needs extensive modeling. A comprehensive overview of the modeling practice for supersonic internal flows can be found in the work of Baurle[10]. The present work will only address the treatment of the mean species reaction rates $\bar{\omega}_s$.

In this work, the RANS equations are solved with the Eilmer[19] open-source CFD package, developed at the University of Queensland. The finite volume solver with explicit time stepping addresses turbulence closure by means of Wilcox's 2006 $k - \omega$ model[20] and has

been previously validated with Eilmer for scramjet type flows [21,22,23], demonstrating similar predictive capability to the more widely adopted k-ω SST model. Shock capturing is ensured by treating the inviscid fluxes with an adaptive method switching between Macrossan's Equilibrium Flux Method (EFM) [24] and Liou and Wada's Advection Upstream Splitting Method combining Difference and Vector splitting (AUSMDV) [25]. With its more diffusive character, the former is active in regions with strong velocity gradients while the latter is used elsewhere. Viscous fluxes are treated by Gauss' theorem and the forward Euler scheme or a predictor-corrector scheme (Heun's method) is used for time integration. Unless otherwise stated the former is selected for time integration as well as the adaptive flux treatment. Eilmer [26] adopts temperature dependent species heat capacities and energies that are evaluated with the polynomial curve fits of McBride and Gordon [27]. An important modeling issue in high-speed turbulent reacting flows is the chemical source term ($\bar{\dot{\omega}}_s$) which is highly non-linear and cannot be directly related to mean flow properties. It is the role of the TCI model to specify this source term. In the following subsection the assumptions of the EDM are introduced followed by the expression for ($\bar{\dot{\omega}}_s$). Thereafter, the limitations of the model are outlined.

2.1 Physical interpretation of the Eddy Dissipation Model

The Eddy Dissipation Model (EDM) was introduced by Magnussen and Hjertager [12,28]. It assumes that fuel and oxidizer are carried by separate eddies in diffusion flames. Furthermore, chemical reactions are fast so that fuel and oxidizer will react as soon as they mix on a molecular scale. Assuming this fast chemistry limit in the EDM, the rate at which reactions occur is then dependent on the rate at which turbulent eddies carrying fuel and oxidizer are brought together. In other words, the mean reaction rate is mainly controlled by the turbulent mixing time. On a dimensional basis, this mixing time is estimated from the integral length scales by using the turbulence model parameters which describe the energy cascade process in turbulent flows. Consequently, the mixing on a molecular level is dependent on the rate at which the eddies dissipate. The model is sometimes referred to as "mixed-is-burned" which highlights the idea that once fuel and oxidizer is mixed, it burns immediately (fast chemistry).

2.2 Implementation of the Eddy Dissipation Model

The EDM is implemented by assuming a single-step irreversible reaction of the form $v'_F F + v'_O O \rightarrow v''_P P$, where v_s are the stoichiometric coefficients of Fuel (F), Oxidizer (O) and Products (P). Such a form is consistent with the model's physical description of fast chemical reactions. It must be noted that the model is limited to scramjet configuration where the chemical time scales are much smaller with respect to the turbulent time scales and is believed to be the case at high Mach regimes. Several CFD studies of generic scramjet combustors, representative for high flight Mach numbers (> 8), documented in the literature, indicate that chemical time scales are smaller than turbulent times scales for the majority of the domain. Locally, such as near the injection, chemical time scales can be of the same order of magnitude as the turbulence time scales [29], i.e. chemical kinetics are important. Depending on the turbulent mixing (injection configuration) the extent of the kinetically dominated region can be limited. The use of a single-step irreversible reaction instead of a reaction mechanism reduces the computational cost and makes it useful for design. In the case of hydrogen combustion,

the reaction is :

$$2H_2 + O_2 \rightarrow 2H_2O \qquad \ldots (5)$$

N_2 acts as an inert species, resulting in four species conservation equations (Equation 4). In EDM, the reaction rate of fuel is defined as:

$$\bar{\omega}_F = -A_{\mathrm{edm}}\, \bar{\rho}\beta^*\omega \, \min\left[\tilde{Y}_F, \frac{\tilde{Y}_O}{s}, B_{\mathrm{edm}}\frac{\tilde{Y}_P}{s+1}\right] \qquad \ldots (6)$$

The oxidizer destruction and product production rates can then be obtained as:

$$\bar{\omega}_O = s\,\bar{\omega}_F \ , \quad \bar{\omega}_P = -(s+1)\bar{\omega}_F \qquad \ldots (7)$$

In the above equation s is the mass stoichiometric ratio defined as $s = (v'_O W_O)/(v'_F W_F)$ and equals 8 for H_2-air combustion [28], W_s is the molar mass in kg/mol and $\tilde{Y}_s$ is the mass fraction. In Equation 6, β^* is a turbulence model constant with a value of 0.09 and ω (1/s) is the specific dissipation of turbulent kinetic energy obtained through the turbulence model. The underlying physical assumption regarding the dissipation of turbulent eddies in the model is accounted for through ω. In summary, the mean fuel reaction rate of EDM, $\bar{\omega}_F(kg/(m^3.s))$, is a function of turbulence (ω), and the mass fractions of fuel ($\tilde{Y}_F$), oxidizer ($\tilde{Y}_O$) and products ($\tilde{Y}_P$) in every cell of the domain.

2.3 Specification of the model constants

Equation 6 requires the specification of two model constants, namely A_{edm} and B_{edm}. In their original work, Magnussen and Hjertager [12] demonstrate the EDM's use on a series of premixed and diffusion flames at low-speed in conjunction with the k-ϵ turbulence model. A setting of A_{edm} = 4.0 and B_{edm} = 0.5 resulted in satisfactory agreement with experimental data (mean temperature, mean composition, mean velocity) for six different test cases. In the literature, the latter setting for the model constants is therefore adopted as the default when using the EDM.

The aforementioned standard setting for the modeling constants might not be the most appropriate for scramjet flow fields. With regard to A_{edm} for instance, Edwards et al. [13] suggest a value between 1 and 4. The physical effect of increasing (decreasing) this constant's value is the promotion (reduction) of the turbulent eddy dissipation process in the flow field which, where available, brings fuel and oxidizer together on a molecular level.

The last term in the minimum evaluation of Equation 6 is intended to account for the effect of hot (or cold) products in a premixed turbulent flame situation where both fuel and oxidizer are contained within the same eddies [12]. The importance of the products on the combustion process can be controlled through the parameter B_{edm}. An increase in the value of B_{edm} will promote the reaction between fuel and oxidizer as more hot products are present to ignite the premixed mixture. The inclusion of the product term implies that, for reactions to occur, an initial product mass fraction is required and is usually taken as: $\tilde{Y}_{P,initial}$ = 0.01. In a scramjet, fuel and oxidizer are injected through different inflows and thus carried by separate eddies which gives rise to a non-premixed combustion process. For this reason, the product term is commonly omitted in their simulation. The present work does therefore not consider the $\tilde{Y}_P$ term in Equation 6.

2.4 Limiting the reaction rate within EDM

The EDM does not include any effect of finite-rate chemical kinetics. Equation 6 does not account for the temperature on the formation of products. Consequently, the EDM has a tendency to over-predict the fuel consumption as well as peak temperatures. The way to mitigate these disadvantages is by limiting $\bar{\omega}_F$ with a kinetic reaction rate. This can be done by use of the reaction rate obtained with the Arrhenius approach (law of mass action) and a single step global reaction[10]:

$$\bar{\omega}_F = \min(\bar{\omega}_{F,\mathrm{edm}}, \bar{\omega}_{F,\mathrm{lam}}) \qquad \ldots(8)$$

where $\bar{\omega}_{F,\mathrm{lam}}$ is given by:

$$\bar{\omega}_{F,\mathrm{lam}} = -v_F' W_F \left(k_f [X_F]^{v_F'} [X_O]^{v_O'} - k_r [X_P]^{v_P'} \right) \qquad \ldots(9)$$

$[X_s]$ is the molar concentration in this definition. The kinetic limit allows the extension of the EDM's applicability to test cases where the combustion is not purely mixing limited but where ignition delay effects are present. However, the trade-off is the introduction of two reaction rate parameters which are not universally defined: the forward reaction rate k_f and the backward or reverse reaction rate k_r. The former is obtained with Arrhenius law by defining a pre-exponential constant A and an activation temperature T_A. Several options are available in the open-literature for the Arrhenius law constants and this work adopts the values A=1.1e19 and T_A = 8052 K as proposed by Chandra Murty and Chakraborty[15]. These values have been obtained for hydrogen combustion by requiring that the flame speed of the single step kinetics match with those from full chemistry as pointed out by Sekar and Mukunda[30]. The k_r is obtained from the forward rate and equilibrium constant. The use of Equation 8 will be referred to as "EDM with kinetic limit". As pointed out by Baurle[10], the use of EDM alleviates the stiffness of the governing equations as turbulent time scales are driving the reactions.

In the case of non-premixed scramjet flow path simulations with EDM, on top of the model constant A_{edm}, values for turbulent Prandtl (Pr_t) and Schmidt number (Sc_t) have to be specified. Including the possibility to limit reaction rates with a kinetic limit, this leaves the user to specify a combination of 3 (or 4) parameters per simulation. Details about the settings and effect of parameter values choices are presented in the following sections.

3.0 TEST CASES

Three generic scramjet combustor geometries are selected to study the application of the EDM, each with a different fuel injection arrangement. The aim is to better understand the choice of the modeling constant A_{edm}. Another aspect of the present investigation is to explore if improvements in the use of the EDM are possible. As the authors' future intention is the use of the EDM in the preliminary design context of scramjet combustors, quantities such as combustion efficiency, total pressure loss and thrust potential[18,31] would be of interest. The latter performance measures are not directly acquired from experimental campaigns. They are however dependent on other quantities which are experimentally obtained such as velocity, temperature, composition and (total) pressure. These experimental

quantities are considered in the present work in order to validate the EDM.

The first test case is the experiment of Burrows and Kurkov[32,33] (Figure 1) where hydrogen is injected parallel to a vitiated air-stream behind a backward facing step. The experimental design results in high combustor entrance Mach number ($>$ 2) and static temperature ($>$ 1000 K), typical for high flight Mach numbers ($>$ 8). A mixing layer is generated close to the injection and a runaway length is observed where the fuel and oxidizer mix before igniting. Whilst the ignition delay is kinetically controlled, it will be demonstrated that once the flow ignites the combustion is mixing limited.

The second test case is the DLR combustor experiment of Waidmann et al.[34] (Figure 11). In this case, hydrogen is injected behind a strut. The physics inside the combustor is dominated by a pattern of shock waves interacting amongst themselves and with shear layers. Turbulence modeling will play a crucial role in capturing the mixing layers and recirculation regions generated behind the strut. These physical features are, in turn, key in controlling the behavior of the flame held behind the strut and the transport of the species along the combustor. A Mach 2 vitiated air stream is supplied to the test chamber with cold temperature ($<$ 1000 K) due to limitations of the facility. Most of the studies reported in the literature on this configuration adopt a TCI which assumes that turbulent time scales are larger than chemical time scales. Waidmann et al.[34] identified the combustion mode to be situated in the flamelet regime. This an indication that, in spite of the cold vitiated air stream conditions, the combustion process is primarily mixing limited. The flamelet and EDM commonly rely on the assumption of that chemical time scales are smaller than mixing time scales. The DLR combustor is therefore adequate for the study of the EDM in this work.

The third test case is the HyShot II combustor[35,36], ground tested at DLR, where fuel is injected perpendicular to the incoming flow inside the constant area combustor. Similar to the experiment of Burrows and Kurkov, the entrance Mach number ($>$ 2) and static temperature ($>$ 1000 K) are representative of a high flight Mach number ($>$ 8). It was demonstrated in several RANS studies[36,37] that the combustion is primarily mixing limited. Moreover, the same comment was made by Larsson et al.[38] in their numerical study of the combustor with LES. The HyShot II combustor is therefore a suitable candidate for study with the EDM. The selected test cases are characterized by different physical features which is suitable for assessing a model's predictive capability over a broader range of supersonic combustion phenomena.

Unit Lewis number is assumed for each species throughout this work and in the case of viscous walls without wall functions, the value of ω is set according to Menter's suggestion for smooth walls[39]. A CFL value of 0.5 is adopted for time integration using the Euler or predictor-corrector scheme. Simulations are converged to a steady state and convergence is monitored through point probes of velocity, density, temperature and pressure at different locations in the computational domains.

3.1 Case 1: Burrows-Kurkov

A commonly used test case in CFD code validation studies for supersonic combustion is the experiment of Burrows and Kurkov[32,33] (BK) shown in Figure 1 for which an extensive set

of comparison data in pure mixing and reacting conditions is available. Many authors have performed RANS studies of the geometry over the last three decades [40,41,42,43,44,45,46]. The test case is known [42,43] to be very sensitive to the the values of turbulent Prandtl (Pr_t) and Schmidt (Sc_t) numbers. During a sensitivity study for the Wilcox k-ω 2006 model, it was observed that the combinations $Pr_t = 0.9$, $Sc_t = 0.5$ and $Pr_t = 0.5$, $Sc_t = 0.5$ gave very similar results in comparison with the experimental data at the exit of the combustor. The value of Pr_t has a significant influence when temperature gradients are high (energy conservation equation), which is mainly the case at the interface between the fuel and vitiated air-stream, hence the limited influence observed in the Burrows-Kurkov configuration. In this study Pr_t and Sc_t were varied between 0.3 and 0.9 [18]. Simulations with the combination $Pr_t = 0.5$, $Sc_t = 0.5$ are presented here. For design purposes, exit properties are used to determine overall engine performance (e.g. combustion efficiency, thrust potential, total pressure loss). The results at the exit location are therefore useful to indicate the usefulness of the model for design analysis.
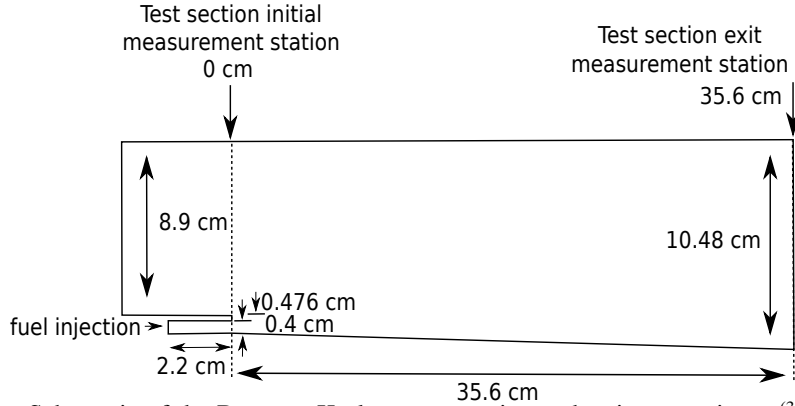
Figure 1: Schematic of the Burrows-Kurkov supersonic combustion experiment [32]. Not to scale.

3.1.1 Problem Formulation

The experimental setup in Figure 1 has been simulated in two stages. This approach was selected in order to considerably reduce the computational cost. The first stage has only to be simulated once as it is not affected by the downstream combustion process. In the first stage, a boundary layer section (BLS) of 65 cm is considered using the same vitiated air supersonic inflow conditions as Edwards et al. [47] listed in Table 1. Note that these values differ from the ones typically encountered in the literature, however Edwards et al. [47] demonstrated a good agreement with experiments in their work, i.e. the peak in total temperature and associated production of H_2O at the combustor exit plane was located similarly to experimental observations. Values for turbulence intensity (I) and the ratio of turbulent to laminar viscosity (μ_t/μ) are set to 5 % and 10 respectively. The exit profile of the first stage is used as an inflow condition for the second stage which considered the geometry depicted in Figure 1 with a BLS of 2 cm. The injector is simulated as a constant area channel of 2.2 cm with conditions in Table 1. Turbulence boundary conditions for the injector are the same as for the separate

BLS simulations. Walls are treated as isothermal at a temperature of 300 K. A supersonic outflow is prescribed where values from the interior of the domain are extrapolated. The simulation results in terms of profiles of total temperature and Pitot pressure are depicted in Figure 2. The profiles are compared to the experimental data collected at the first section (x = 0 cm) as well as to the CFD of Edwards et al.[47] obtained with a hybrid RANS / LES approach. An overall satisfactory prediction of the inflow conditions are observed with a boundary layer thickness at the entrance of the combustor around 1 cm.

Table 1: Inflow and injector flow conditions for Burrow-Kurkov' experiment.

	inflow	injector
u (m/s)	1741.4	1217.0
T (K)	1237.9	254.0
p (Pa)	96000.0	101350.0
Y_{H_2} (-)	0.0	1.0
Y_{O_2} (-)	0.258	0.0
Y_{H_2O} (-)	0.256	0.0
Y_{N_2} (-)	0.486	0.0

(a)

(b)
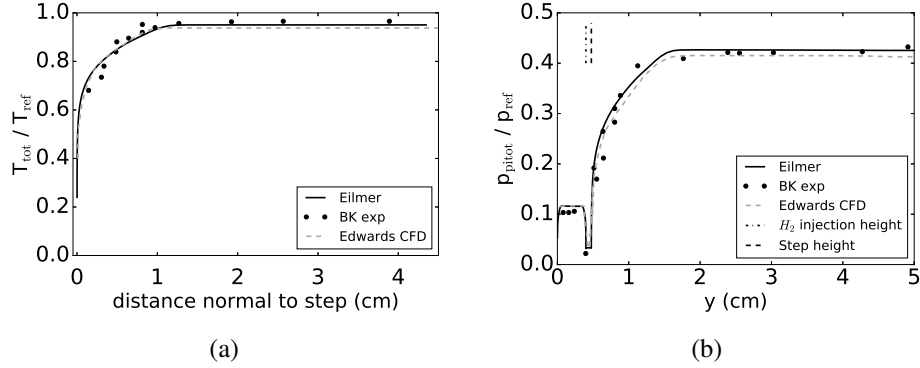
Figure 2: Vitiated air flow total temperature (a) and Pitot pressure (b) at the entrance of the combustor. T_{ref}=2380 K, p_{ref}=17.1e5 Pa

For the second stage calculation, a mesh independence study has been performed with structured grids containing 129 987 (mesh 1) and 185 920 (mesh 2) cells. In both cases, the maximum first cell distance to physical walls was below 5e-6 m. The EDM with setting A_{edm} = 4 was adopted. The result of the mesh refinement study on the total temperature (T_0) at the exit of the combustor (x = 35.6 cm) is shown in Figure 3. The horizontal axis represents the distance from the lower wall. No visible differences in predictions are observed indicating mesh independent results. The same is valid for the combustion efficiency along the combustor. This paramater has been computed according to Kim et al.[48] as :

$$\eta_c(x) = 1 - \frac{\int \rho u Y_F dA}{(\int \rho u Y_F dA)_{x=0}} = 1 - \frac{\dot{m}_F}{(\dot{m}_F)_{x=0}} \qquad \dots (10)$$

Equation 10 evaluates the mass flow rate of fuel ($\dot{m}_F$) across a plane at any position with respect to the injected amount. The profiles of η_c obtained by both meshes are very similar (< 6 K for T_0 and < 0.1 % for η_c) and a mesh independent result is achieved. In the following discussion, the finer mesh is considered.
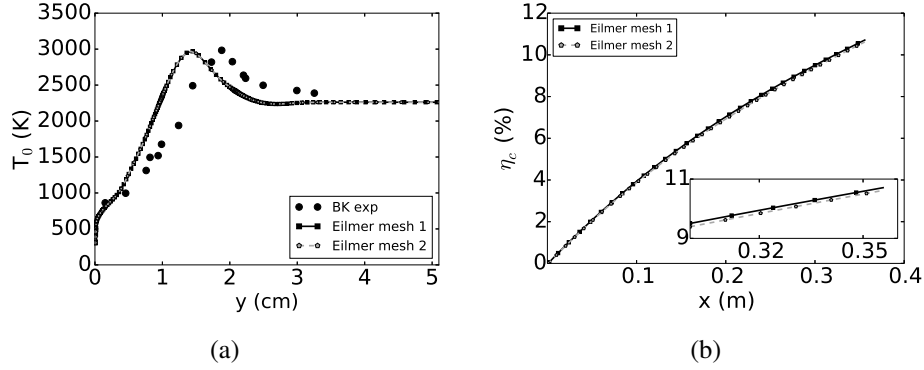

Figure 3: Predictions of total temperature at x=35.6 cm (a) and combustion efficiency (b) obtained with different mesh sizes.

3.1.2 Results

The influence of the A_{edm} parameter is assessed through comparison with the available experimental data measured at the exit plane (x= 35.6 cm) in Figures 4 to 6 for Mach number, total temperature, Pitot pressure, mass flow rate and composition. The horizontal axis represents the vertical distance from the lower wall. Simulations have been performed with several values of the A_{edm}. No kinetic limit has been used in these results. It will be shown hereafter that it did not influence the different profiles at the exit of the test section.

The effect of varying A_{edm} is observed in the profile of total temperature (T_0) in Figure 4. A higher peak temperature corresponds to a higher A_{edm} . This behavior is a direct consequence of the model (Equation 6) as more products are allowed to form which in turn increases mean temperature. A value of 6 results in a peak value of T_0 comparable to experiments, however its location is closer to the lower wall by ≈ 0.44 cm (4.2 % of the exit height). An increase of A_{edm} = 4 above its standard value of 4 does not demonstrate drastic changes which suggests the presence of an asymptotic limit. This is explained by the scarce presence of reactants available for reaction at that location (Figure 6b, y ≈ 1.5 cm). Experimentally this situation occurs further away from the wall. Adopting a lower value of the model constant (A_{edm} = 1) results in a consistent under-prediction of the peak total temperature. Regarding the profiles of Mach number (Figure 4a) , a higher A_{edm} setting is in better agreement with the experimental data. Overall a good match with experiment is observed for Mach number. Figure 5, showing Pitot pressure (p_{pitot}) and mass flow, confirms the need for a higher value of the EDM constant in order to get an improved agreement with experiments. The influence is, however, contained to the region closer to the wall (y < 2 cm).
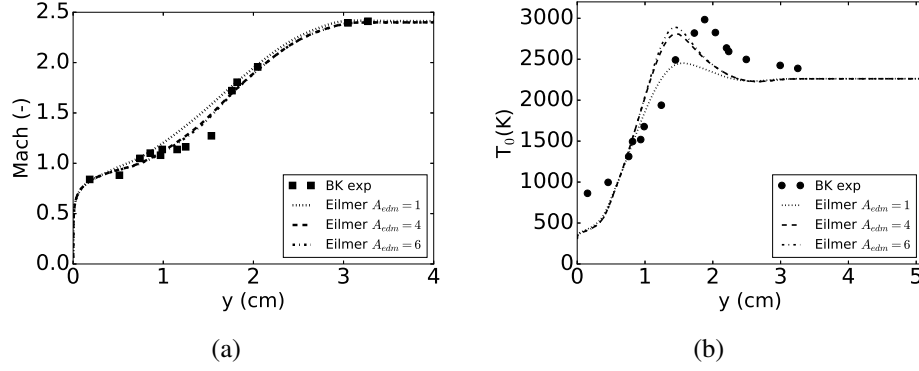
Figure 4: Predictions of Mach (a) and total temperature (b) at x=35.6 cm obtained with EDM compared with experimental values of Burrows and Kurkov.

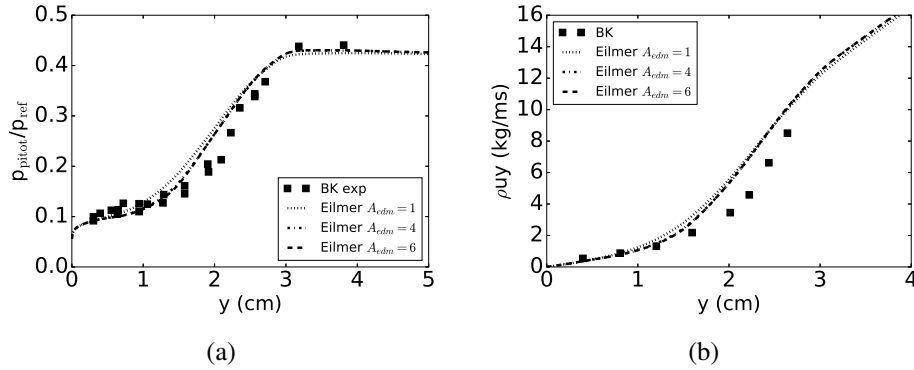Figure 5: Predictions of Pitot pressure (a) and mass flow (b) at x=35.6 cm obtained with EDM compared with experimental values of Burrows and Kurkov. P_{ref}=17.1e5 Pa

Figure 6 shows the exit profiles of species mole fractions of H_2O and O_2. The observations on the effect of A_{edm} on the H_2O mole fraction are in agreement with the total temperature curves discussed previously. A higher A_{edm} setting predicts peak values comparable to experiment but an offset in peak position is present. The different EDM results under-predict the penetration depth of hydrogen into the vitiated airflow. The X_{O_2} profiles show that the experimental slope is better captured by a higher value of the EDM constant.

Overall the best results with EDM are obtained by prescribing A_{edm} = 6. With the latter setting, a relative error in peak total temperature and peak product mole fraction of respectively 3.5 % and 4.1 % is observed. The standard value for the same model constant results in relative errors of 6.2 % and 7.6 % for these peak quantities. The explanation for this result can be understood by studying the contour of product mass fraction $Y_P = Y_{H_2O}$
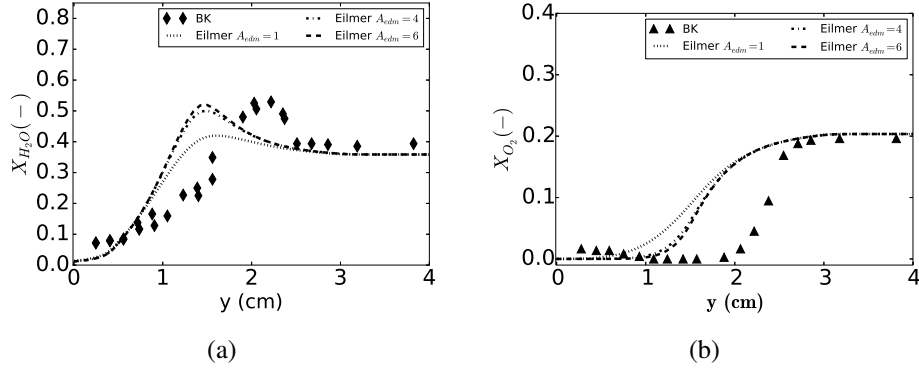
Figure 6: Predictions of H_2O (a) and O_2 (b) mole fraction at x=35.6 cm obtained with EDM compared with experimental values of Burrows and Kurkov.

(or mean temperature) and ω. Figure 7 shows the product mass fraction contour predicted by the EDM (upper representation). The top contour is in accordance with what would be obtained with a single-step reaction (see[49]) except for the fact that combustion occurs very close to the injection point. The latter behavior of not predicting any ignition delay is unphysical. It is however expected as the EDM allows products to be formed as soon as fuel and oxidizer mix. Introducing the kinetic limit (Equation 8) mitigates this effect as can be seen in the bottom contour. It was mentioned earlier that applying this limit does not affect the CFD predictions at the exit of the combustor. This statement is confirmed by observing the profiles of Mach number and total temperature in Figure 8. The same observations are valid for the other quantities and are therefore not shown in this work. The kinetic limit only affects a very small region near the injector and the length of the combustor is long enough to allow the EDM to compensate this localized effect near the injector. That is, downstream the point of fuel injection the combustion products that couldn't be formed earlier will rapidly form. The minimal influence of the kinetic limit is explained by the high vitiated air-stream temperature. In the experiments, ignition onset is indicated by a rise in wall static pressure 18 cm downstream of the injection point[33]. With the kinetic limit, this occurs at $\approx$ 1 cm downstream of the injection point.

The EDM assumes that a higher mixing rate is characterized by a higher value of ω. This assumption is not valid near the injector where no combustion takes place but where very high values of ω are predicted by the turbulence model in Figure 9. Note that high values of ω are relative to the rest of the flow field. In the shear layer near the backward facing step, ω is an order of magnitude larger than at the fuel/oxidizer interface near the exit of the combustor. Moving further away from the injection point, a decrease in ω is observed in Figure 9 which is coupled to a decay in the strength of the turbulence inside the combustor. The high local values in the shear layer near the injector causes an early product formation. In reality the combustion should start after some ignition delay. The location for ignition onset is downstream of the injection point where the value of omega decreases. Consequently, an increase in the A_{edm} constant is required as compensation. Values higher than 6 have no strong influence as there are not enough reactants at stochiometric ratio left to burn at the interface
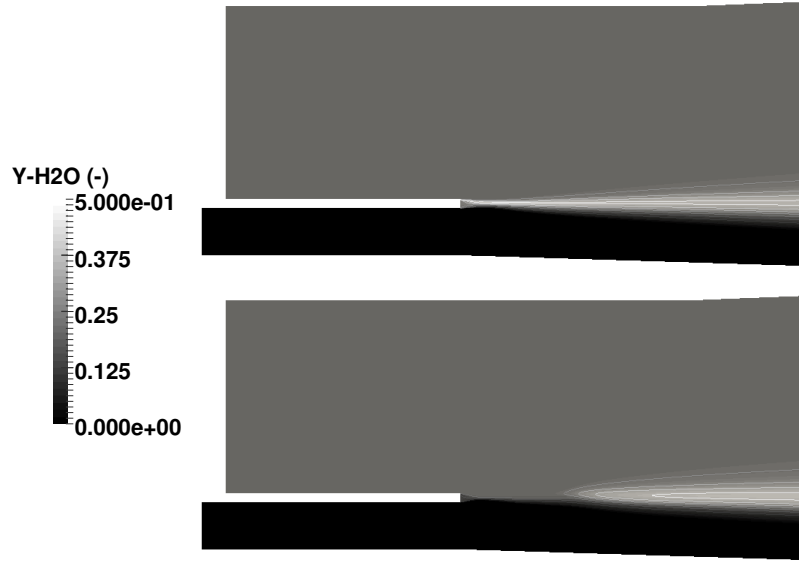
Figure 7: Mass fraction contours of H_2O close to the injection point with from top to bottom: EDM and EDM with kinetic limit.
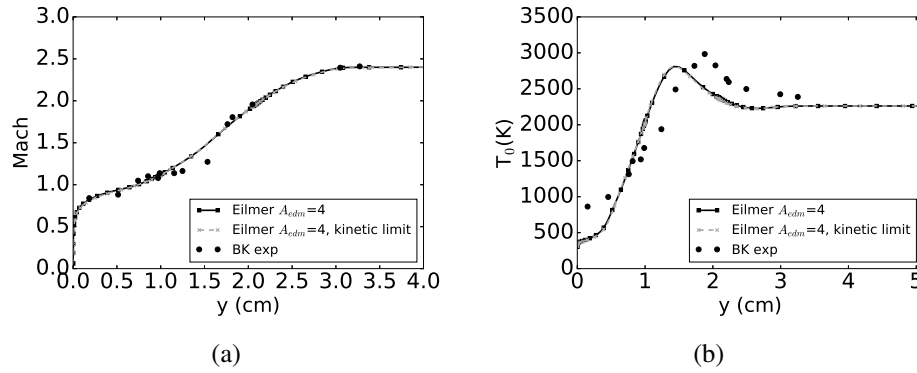

(a) (b)

Figure 8: Comparison of EDM with and without kinetic limit on Mach (a) and total temperature (b) at the exit of the combustor (x = 35.6 cm)

between the fuel stream and the vitiated air stream.

Ignition Delay with Zonal EDM

Figure 7 demonstrates that the kinetic limit is perhaps not the most adequate way of introducing an ignition delay in a shear layer environment with high free stream temperature. Its effect is minimal and is far from representative of what is experimentally observed.
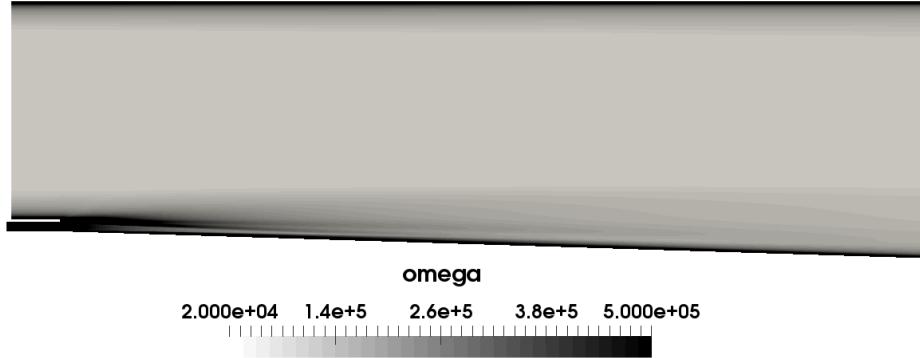
Figure 9: Contour of ω for the experiment of Burrows and Kurkov

Moreover, the combustion induced shock wave, reported by Bhagwanding et al.[49], is not predicted by the EDM. The reference work of Burrow and Kurkov[32] mentions that it is possible to rely on a one-dimensional kinetics program to obtain an estimate of the expected ignition delay. Such an approach can be very beneficial for the use of the EDM, which lacks the ability to account for ignition delay in a parallel injection setting with high free stream temperatures (above autoignition temperature of hydrogen), as shown here. Based on a free stream temperature of 1270 K, an H_2/O_2 ratio of 0.013 and a free stream mixture containing N_2, O_2, H_2O and NO, an induction time (or ignition delay or runaway length) of 90e-6 s was obtained[32] with the one-dimensional kinetics program developed by Bittker and Scullin[50]. Using an averaged vitiated air stream velocity at the entrance of the combustor of 1689 m/s (obtained from CFD), a flow residence time equal to 2.1e-4 s is obtained. From the averaged velocity value and the previously calculated induction time, the ignition location inside the combustor is estimated to be at x = 0.153 m. Note that this approach only gives a rough estimate of the induction process. It does not, for example, account for the low fuel stream temperature near the wall which can have a significant influence as indicated by Burrows and Kurkov[32]. Nevertheless, this information can be relied on for a better use of the EDM.

A simulation has been performed relying on the above ignition delay estimate where no combustion is allowed at any axial location before that point, hence the terminology "zone". Recall that, experimentally[33], an ignition delay is observed between 18 cm (wall pressure trace) and 25 cm (photographs of OH radiation). Numerical predictions have also been obtained with finite-rate chemistry simulations (no TCI) relying on the 7 species, 8 reactions mechanism of Evans-Schexnayder (E-S)[40] with modified third-body efficiencies in accordance with Bhagwandin et al.[49] The finite rate chemistry (FRC) simulation predicted an onset of ignition at a position of 23 cm. This value is located between the experimentally observed interval mentioned previously showing that the chemical kinetics are well reproduced by the selected reaction mechanism.

Figure 10 compares the different approaches (EDM, EDM-zonal, FRC) with experimental values of Mach number and total temperature (T_0) at the combustor exit. The classical EDM is shown for a constant value A_{edm} = 6 following the parametric study discussed previously. The profiles of T_0 show that the use of the EDM can be greatly improved with an estimate

of ignition onset. A good agreement with experimental T_0 values are observed near the wall with the zonal use of the EDM. The relative error with respect to the experiment is ≈ 1.5 % for the peak value and ≈ 1.1 % for the peak location in Figure 10a. The FRC (E-S) predictions result in relative errors of ≈ 2.0 % and ≈ 13.2 % for respectively the peak T_0 value and location. These quantities are ≈ 3.5 % and ≈ 23.8 % for the classic EDM. Therefore, the FRC does perform better than the classic EDM but slightly less than the zonal EDM. This is explained by the fact that the combustion process is kinetically limited until the onset of ignition whereafter it becomes mixing-limited. The same observation was made by Kirchhartz et al.[51] in an axisymmetric scramjet combustor with similar fuel injection mechanism. The EDM assumes a mixing limited combustion and is therefore more appropriate once the flow is ignited. In terms of the Mach number profile (Figure 10b), a lesser agreement with experimental data is observed for the EDM with ignition estimate compared to the curve without. Nevertheless, it remains superior to the FRC CFD prediction in the vicinity of the wall (y < 1 cm). The observations for the profiles of Pitot pressure are similar to the Mach number and the composition profiles are in close agreement with the curves for T_0. They are therefore not shown here.

(a)   (b)
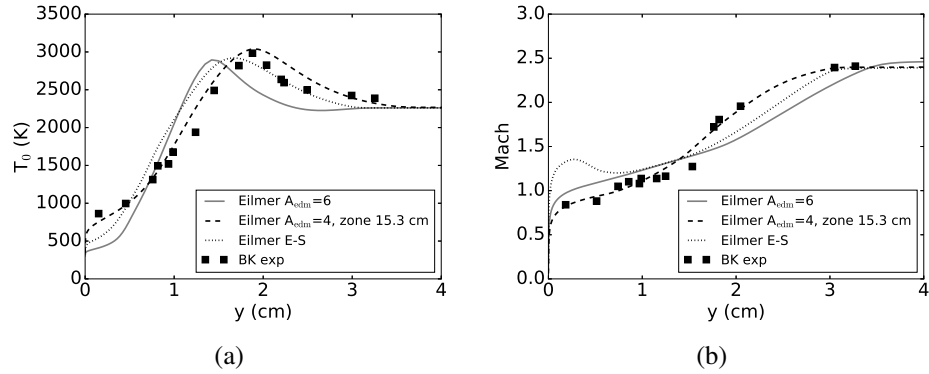
Figure 10: Comparison of EDM with and without zone on total temperature (a) and Mach number (b) at the exit of the combustor (x = 35.6 cm).

In conclusion, even though the estimated induction length from the one-dimensional program does not agree with experimental observations [†], it proves to be very useful information for an improved use of the EDM. The zonal EDM provides improved results in T_0, Mach number, Pitot pressure and composition profiles with respect to the classic EDM. It is therefore a viable approach for study of similar scramjet configurations.

[†] It must be noted that the BK test case is sensitive to the selected turbulence model[43], inflow conditions[43] and reaction mechanism[49]. Moreover, there is some experimental uncertainty regarding the onset of ignition (18 cm < $x_{ignition}$ < 25 cm).

3.2 Case 2: DLR combustor

The DLR combustor experiment of Waidmann et al.[34] is depicted in Figure 11. Similar to the Burrows-Kurkov experiment, measurements have been taken in both a pure mixing and a combusting setting. The main geometry is notionally two-dimensional, however the use of porthole injectors on the rear of the strut sets up an inherently three-dimensional flow field. Several two-and three-dimensional RANS studies of this combustor test case can be found in the literature[52,53,16,54,55,56] where each author introduces a TCI model. In spite of the three-dimensionality of the configuration, two-dimensional studies are useful as a proof of concept for modeling techniques. Oevermann[52] and Mura et al.[53] obtained reasonable results in their two dimensional studies. Following this approach, the present work considers the application of EDM on a two-dimensional domain with single slot injector. It is expected that the two-dimensional assumption will introduce a certain degree of error when making direct comparison to experiment. However, Gao et al.[54] demonstrated little differences ($\approx$ 50 K) in axial temperature profiles between two-and three-dimensional simulations adopting a flamelet combustion model. Three-dimensional simulations of the present setup have to be considered for future work in order to quantify the errors introduced by a two-dimensional assumption.
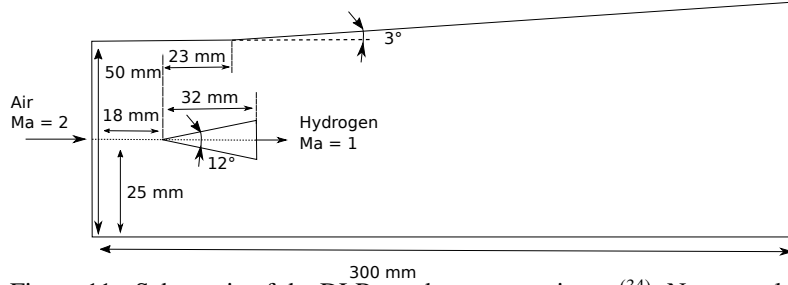

Figure 11: Schematic of the DLR combustor experiment[34]. Not to scale.

3.2.1 Problem Formulation

A structured grid was generated for the domain shown in Figure 11. The distance between the supersonic inlet, with conditions given in Table 2, and the start of the strut is 18 mm and the total combustor length is 300 mm. Upper and lower walls are treated as inviscid which is an acceptable choice given the distant location with respect to the reaction zone. The strut walls are defined as adiabatic and a supersonic outflow is assumed. Given the relatively low stream temperatures in the combustor and the location of the reaction zone further downstream of the strut, the heat transfer to the strut walls is expected to be small supporting the adiabatic wall boundary condition setting. Turbulence quantities are taken similar to Oevermann[52] and Mura et al.[53]: for the free stream inflow $I = 0.3\%$, $\mu_t/\mu = 675$ and for the injector $I = 3.3\%$, $\mu_t/\mu = 63$.

A mesh independence study has been performed with structured grids containing 117 000 (mesh 1) and 276 432 (mesh 2) cells. For this study, the EDM with setting $A_{edm}=4$ and a combination $Pr_t = Sc_t = 0.9$ was adopted. The result is shown in Figure 12 for the

Table 2: Inflow and injector flow conditions for the DLR combustor experiment.

	inflow	injector
u (m/s)	730.0	1200.0
T (K)	340.0	250.0
p (Pa)	100000.0	100000.0
Y_{H_2} (-)	0.0	1.0
Y_{O_2} (-)	0.232	0.0
Y_{H_2O} (-)	0.032	0.0
Y_{N_2} (-)	0.736	0.0

horizontal velocity component along a line superimposing the symmetry axis of the strut. In the following discussions, the term centerline velocity will be used instead. Some small differences are observed in the recirculation regions behind the strut ($x \approx 70$ mm) as well as further downstream in the combustor. However, for most of the profile both meshes predict the same centerline velocity. Also shown in Figure 12 is the combustion efficiency computed with Equation 10. The profiles are very similar with a maximum difference of 1.5 % between the grids. Given the limited effect of the refinement ($\approx$ factor 2) on the solution, the coarser mesh is suitable to study the application of the EDM on the combustor. Therefore the following discussion considers the first mesh.
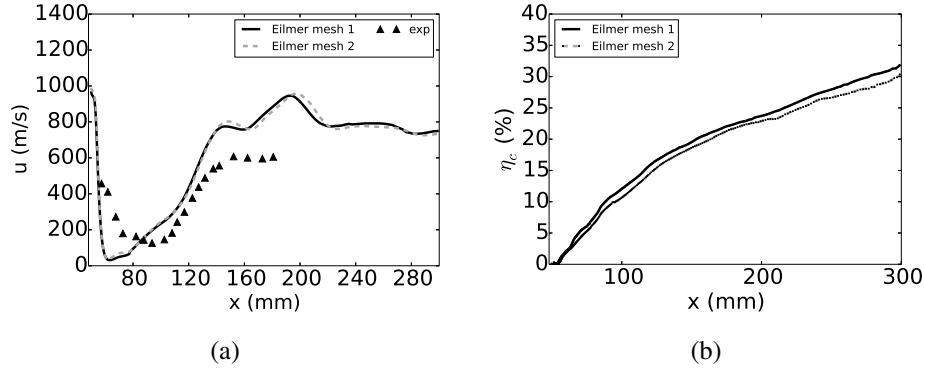

Figure 12: Predictions of centerline velocity (a) and combustion efficiency (b) obtained with different mesh sizes.

3.2.2 Results

The DLR combustor test case has proven to be very challenging to predict in a two-dimensional context. Multiple combinations of the different settings for A_{edm}, Pr_t and Sc_t were explored and only a limited number of results will be discussed in this paper. Waidmann et al.[34] collected, inter alia, data on axial velocity and temperature at the cross-sections marked with 1 and 2 in Figure 13.

Firstly, the effect of introducing a kinetic limit on the EDM reaction rate has been explored. Figure 14 shows its influence compared with some of the available experimental data for the EDM setting, $A_{edm} = 4$, and a turbulent setting of $Pr_t = Sc_t = 0.9$ in accordance with Gao et al.[54] Simulations with kinetic limit were initiated from the converged EDM result without limit as to avoid the need for a source of ignition given the low free-stream temperatures.
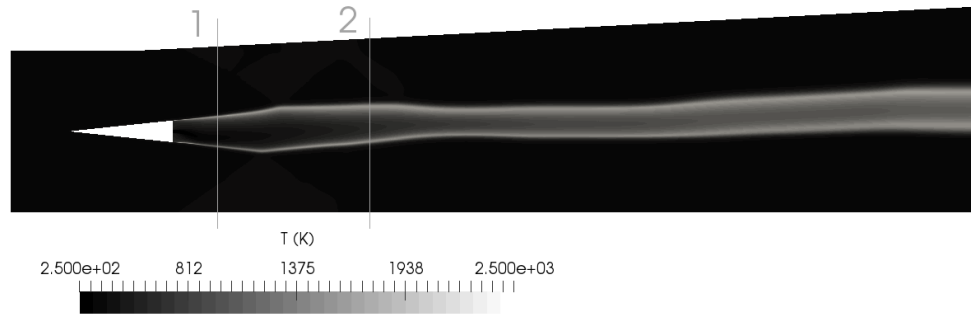

Figure 13: Temperature contour ($A_{edm} = 4$,$Pr_t = Sc_t = 0.9$) with indication of the axial measurement locations considered in the present work.

Axial velocity profiles did not show significant differences however the temperature profiles did. This behavior is observed in Figure 14 (b) where the axial velocity is presented at the second measurement location of Figure 13. Applying the kinetic limit mostly affected the local minimum in axial velocity between the two shear layers but its position is not influenced by the modeling option. The EDM with kinetic limit shows an under-prediction of the minimum axial velocity whilst the classic EDM over-predicts the experimental value. Despite having similar minimum locations, the velocity profiles of the simulation are not aligned with experimental trends. It must be noted that even the more advanced CFD models[57,58,59] do not yield a good agreement with the mean axial velocity at location 2, i.e. the minimum location is wrongly predicted. This observation demonstrates the challenging nature of this test case. It is not exactly clear what the reasons are for this but a possible cause could be inaccuracies in the recirculation regions prediction as pointed out by Genin and Menon[57].

The numerical results of the axial temperature profile are strongly influenced by the kinetic limit. Predictions at the first measurement station shown in Figure 13 are presented in Figure 14 (a). Applying the kinetic limit suppresses combustion in the lower recirculation region just downstream of the strut. This results in a single temperature peak which does not agree with the experimental data. The observation is explained by the low free stream temperature and the asymmetry in the geometry. The EDM results in peak temperature locations similar to experiments and the reference CFD. The structure of the recirculation regions are however different in the numerical simulation. Figure 14 (c) shows the centerline velocity. The end of the strut is located at x = 64 mm in this representation. As mentioned above, the

structure of the recirculation regions behind the strut are different depending on whether EDM is used with a kinetic limit or not. The upper recirculation zone extends down to the centerline which is not experimentally observed, neither predicted by the standard EDM (see positive values for u in Figure 14 (c)). Further downstream the combustor, the velocity profile of the EDM with kinetic limit is in better agreement with the experimental data than the other profiles. The kinetic limit is not applied in the following discussion as the influence of this limit in the region close to the strut results in worse agreement with the experimental data.
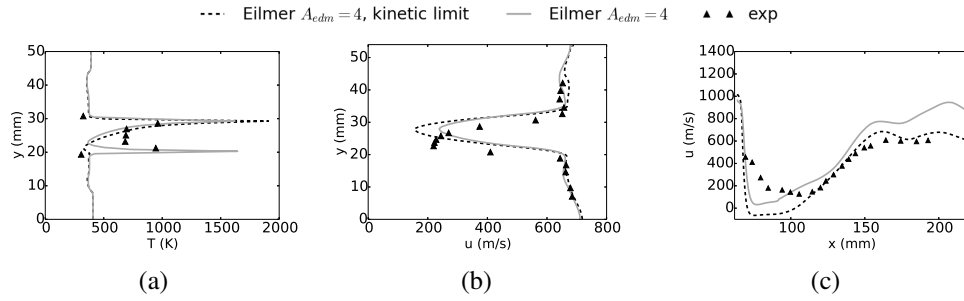

Figure 14: Effect of applying the kinetic limit on the temperature at axial location 1 (a), the velocity at axial location 2 (b), the centerline velocity (c). $A_{edm} = 4$, $Pr_t = Sc_t = 0.9$.
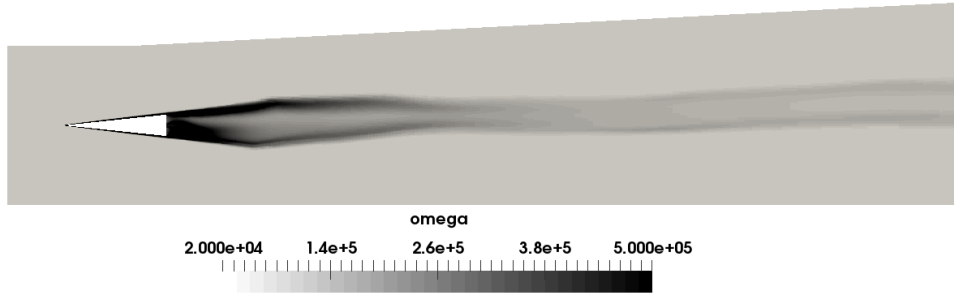

Figure 15: Contour of ω for the DLR combustor experiment of Waidmann et al.[34]

Secondly, the most appropriate setting for the A_{edm} constant is now investigated. From the observations in the Burrows-Kurkov test case, the configuration is expected to have high values of ω in the shear layers induced by the strut with decreasing strength towards the end of the combustor. Figure 15 confirms this statement. Moreover, the higher ω values are present near the fuel injector. Experimentally, the flame is located in the vicinity of the injection point behind the strut. In contrast to Burrows-Kurkov, there is no significant runaway length, i.e. combustion does occur almost as soon as fuel and oxidizer mix. In terms of the EDM, given the high ω values behind the strut, a relatively low value of A_{edm} should be applied. Too low a value would however negatively influence the combustion zone further downstream characterized by lower ω values. Figure 16 shows the mean temperature at locations 1 and 2 of Figure 13 as well as along the lower combustor wall obtained with the

same three settings of the EDM as in Burrows-Kurkov, namely A_{edm}= 1, 4 and 6. Figure 17 presents the velocity at the same locations 1 and 2 as above as well as the centerline velocity. The influence of A_{edm} on the velocity is very limited: minimal at the axial measurement locations and slightly more pronounced along the centerline. There is an influence on the size of the upper recirculation zone directly behind the strut. Regarding the lower wall pressure, a different A_{edm} setting does not strongly affect the profile. This can be understood from the fact that the width of the reaction zone along the combustor is not influenced by the combustion model which is shown in the temperature profiles. It is however influenced by the interaction between the shock waves and the turbulent shear layers, and consequently by the turbulence model. The wall pressure trends are similar, i.e. shock reflection locations, to the hybrid RANS/LES reported in the literature by Potturi and Edwards[58] (see Cases 1 to 4 in Figure 12). The width of the reaction zone (Δy_{reac}) predicted by Eilmer with different EDM settings is comparable to the experimental measurements. From Figure 17b, the CFD predicts a value for Δy_{reac} of $\approx$ 15.5 mm and the experimental data a value of $\approx$ 13 mm.

At the first measurement location, the mean temperature follows the experimental trend well. Peak values in the two shear layers are strongly influenced by the A_{edm} setting. It is difficult to state which setting is more appropriate as not enough experimental data points are available in the shear layer to shed light on the observed peak temperature values. It is inferred that a value for A_{edm} higher than 1 and below 4 is required. Adopting A_{edm} = 1 results in an under-prediction of the peak mean temperature in the lower shear layer at the first measurement location. At the second location, the same effect of the EDM setting is observed: higher value coupled with increased peak temperature. In order to match the experimental peak, A_{edm} should be set to $\approx$ 4. However, a double peak profile is predicted by the CFD which is not experimentally observed. Gonzalez-Juez et al.[60] mentioned in a review paper that a similar observation has been reported in the literature in an LES study with the Eddy Break Up (EBU) model for TCI treatment. The latter model is closely related to the EDM. Nevertheless, the observations are in accordance with the above stated expectations of the EDM: in the vicinity of the strut (a region with higher values of ω) a lower A_{edm} setting is more appropriate while further away (a region with lower values of ω) a higher A_{edm} setting performs better. Overall the standard setting of 4 is a good compromise for the DLR combustor as it provides a reasonable comparison with the experimental data at the different locations inside the combustor.
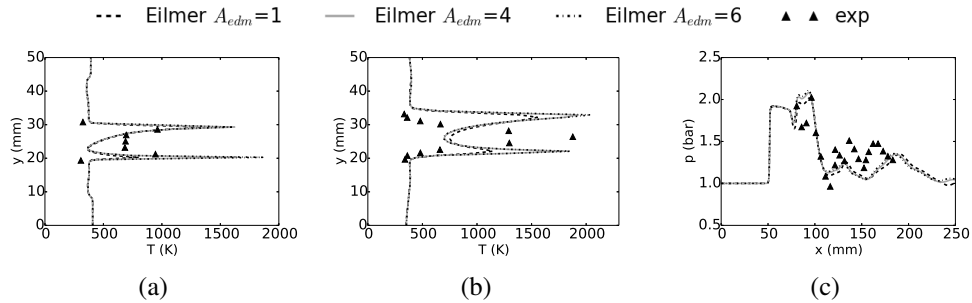

Figure 16: Effect of the model constant A_{edm} on the temperature at axial locations 1 (a) and 2 (b), and on the wall pressure (c). Results obtained with $Pr_t = Sc_t = 0.9$.
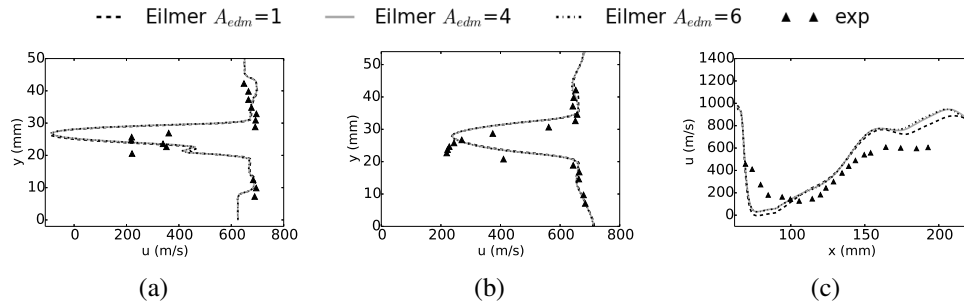
Figure 17: Effect of the model constant A$_{edm}$ on the velocity at axial locations 1 (a) and 2 (b), and on the centerline velocity (c). Results obtained with $Pr_t = Sc_t = 0.9$.

3.3 Case 3: The HyShot II combustor

The HyShot II combustor was designed for a Mach 8 flight test experiment on supersonic combustion[35,36]. Experimental campaigns have been undertaken in the HEG Shock tunnel of the DLR with a 1:1 scale representation using hydrogen fuel. The configuration has been studied with different RANS approaches in the literature[35,36,37]. A detailed description of the ground test experiment is given by Karl[36] and is considered for numerical study in the present work.

3.3.1 Problem Formulation

This simulation is performed in three dimensions. Only a part of the combustor, shown in Figure 18, is considered for application of the EDM. It consists of half an injector and two symmetry planes. The considered computational domain size contains sufficient experimental data points in order to analyse the EDM and the effect of the model constant (A$_{edm}$). The computational domain is discretized in $\approx$ 2.8M hexahedral cells and an O-grid topology is adopted for the injector. Pecnik et al.[37] obtained satisfactory reacting wall pressure traces with a structured grid consisting of 2.6M cells. Moreover, the injector was modeled as part of the computational domain which extended to include a part of the nozzle. This suggests that the current mesh size of 2.8M cells is a good starting point. In order to ascertain the suitability of the grid for the Eilmer CFD solver, future work should include a mesh independence study.

The injector is modeled as a supersonic inflow boundary with conditions: w = 1206.7 m/s , p = 263720 Pa, T = 249 K, I = 5 %, μ_t/μ = 10. The resulting equivalence ratio is 0.29. The upper and lower boundaries (z ordinates) are treated as viscous isothermal walls at a temperature of 300 K. Compressible wall functions of Nichols and Nelson[61] are adopted so as to reduce the computational cost of the simulation due to grid requirements . The two-dimensional CFD inflow conditions of Karl et al.[35,36] are prescribed at the inlet of the three-dimensional domain (same inflow for each lateral cell location) and correspond to averaged conditions: T = 1300 K, p = 130 kPa, u = 1720 m/s and Mach = 2.4. The boundary layer (BL) along the upper wall (cowl side) is assumed to be fully turbulent while a transition

from laminar to turbulent flow takes place at the lower wall (injector side) around x = 45 mm. This is accounted for in Eilmer by generating two turbulent zones across the width of the domain, shown in Figure 18. Outside these zones the turbulent quantities (k,ω) are purely transported and do not affect the other governing equations.

Inviscid fluxes are treated with the AUSMDV and time stepping with a predictor-corrector scheme. Values for turbulent Prantl and Schmidt numbers are set to 0.9 and 0.7 respectively. Sensitivity studies to these parameters have been reported by Karl[36] and Pecnik et al. [37] with the Spalart-Allmaras and the k-ω SST turbulence model respectively. It was observed by both authors that the resulting pressure traces with different model parameters remain between the experimental uncertainty of the measurements. Therefore, such a sensitivity with the k-ω 2006 model is not considered in the present work. Instead, the standard setting for these parameters is selected.
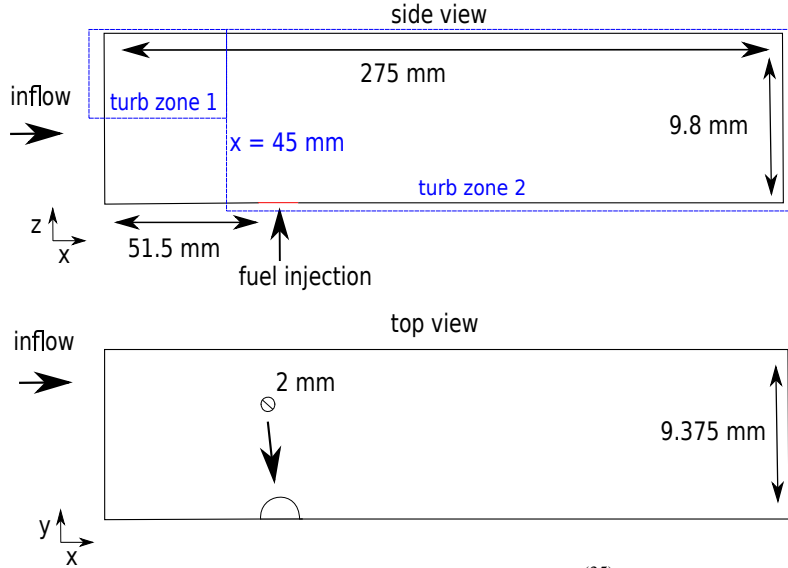

Figure 18: Schematic of the HyShot II combustor[35]. Not to scale.

3.3.2 Results

Reacting simulations of the HyShot II combustor have been performed with the EDM. It was not possible to converge toward a steady-state. It is likely there is an inherent unsteadiness in the flow that has been resolved by the explicit time stepping, hence it is an unsteady (URANS) simulation. URANS requires small enough time steps in order to capture variations in mean flow properties due to the largest turbulent fluctuations. Karl et al. [62] reported a study of the unsteady shock train inside the HyShot II combustor. The authors applied URANS with a second order accurate temporal discretization scheme and physical time steps of 1e-7s. The predictor-corrector scheme used in Eilmer is second order accurate[63] and time steps in current HyShot simulations were below 4e-9 s following the evaluation of the CFL criterion. Time steps in current work are orders of magnitude smaller than in the CFD simulations of

Karl et al.[62] It can therefore be concluded that an inherent unsteadiness in the flow field is expected to be captured and that URANS is performed in the present work. Note that the non-reacting simulations did converge to a steady state. It is inferred that the unsteadiness originates due to the interaction between air flow and injected fuel (shear driven instability) and / or the combustion process. In order to enable comparison with experiments, the CFD data is time-averaged over two flow lengths once initial transients have passed which is suitable for design estimations.

The effect of varying the value of A_{edm} on the wall pressure is investigated in Figures 19 and 20. Increasing the value results in increased pressure values and an overall vertical shift of the profile. This effect is more pronounced when comparing the curves of $A_{edm} = 4$ and 6 with respect to the curves of $A_{edm} = 2$ and 4. On the injector side in Figure 20, an upstream shift of the shock reflection positions is induced by an increased A_{edm} value. The cowl wall pressure trace is in good agreement with the experimental data for any choice of A_{edm}. On the injector side, the pressure traces are within the experimental uncertainty for most of the combustor length. Close to the axial injection location (≈ 52.5 - 120 mm), the EDM is unable to account for the experimental pressure variation. A similar observation is made for the CFD predictions obtained by Karl[36] which are shown in Figure 21 (b). The reference CFD results are predicted by the Tau code with the Spalart-Allmaras turbulence model in conjunction with a no-model chemistry (modified Jachimowski mechanism) approach. The same Pr_t and Sc_t settings used in Tau-based analysis are used in this work. Note that Pecnik et al.[37] showed more success in capturing the injector side wall pressure trace with a flamelet TCI model in conjunction with the k-ω SST turbulence model. On the cowl side (Figure 21 (a)), the EDM pressure trace demonstrates a similar trend to the reference CFD. In terms of shock strength, $A_{edm} = 6$ agrees better with Tau. The pressure profiles in Figures 19 and 20 have been integrated to obtain the pressure force and averaged pressure. The same averaging has been performed for the experimental values with results shown in Table 3. Given the limited amount of experimental measurements, the averaged quantities should be seen as relative indication rather than an absolute reference point. The Exp_{min} and Exp_{max} are calculated based on the error bars. On the injector side, the pressure force calculated with the different EDM simulations over predict the experimental maximum. This result is probably due to the pressure prediction between ≈ 52.5 - 120 mm and the lack of experimental data in this region. Nevertheless, in terms of averaged pressure, simulations with different A_{edm} settings are within the experimental bounds. On the cowl side, the same observation is made as for the injector side with regard to the averaged pressure values. The pressure force computed for $A_{edm} = 2$ and 4 are within the experimental bounds while it is overestimated for $A_{edm} = 6$.

Table 3: Averaged pressure and pressure force predicted by the EDM for the HyShot II combustor.

	Exp_{min}	Exp_{avg}	Exp_{max}	$A_{edm} = 2$	$A_{edm} = 4$	$A_{edm} = 6$
Injector wall						
pressure force (kN)	39.4	45.0	50.4	52.5	53.0	54.5
averaged pressure (kPa)	162.5	185.7	207.9	190.1	192.7	198.2
Cowl wall						
pressure force (kN)	43.3	48.3	53.9	52.7	53.1	54.7
averaged pressure (kPa)	170.1	189.7	211.9	191.5	193.1	198.8

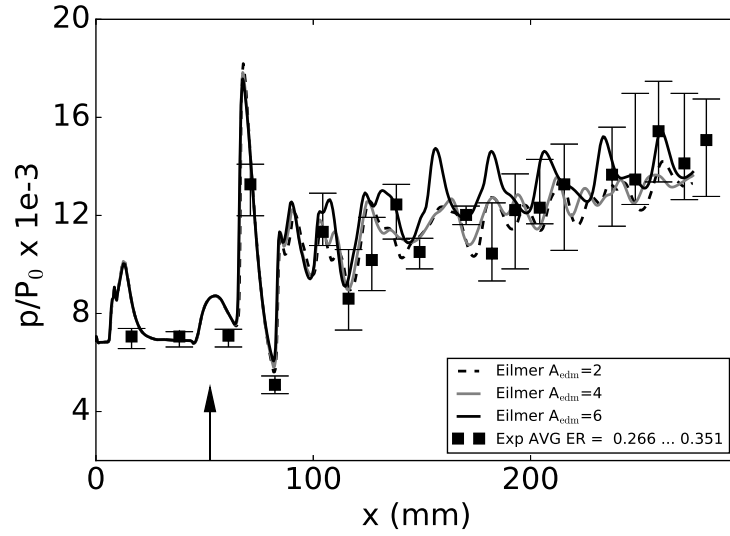Figure 19: Effect of A_{edm} on the time-averaged pressure traces along the cowl wall at y = 9.375 mm with P_0 = 17.73 MPa.
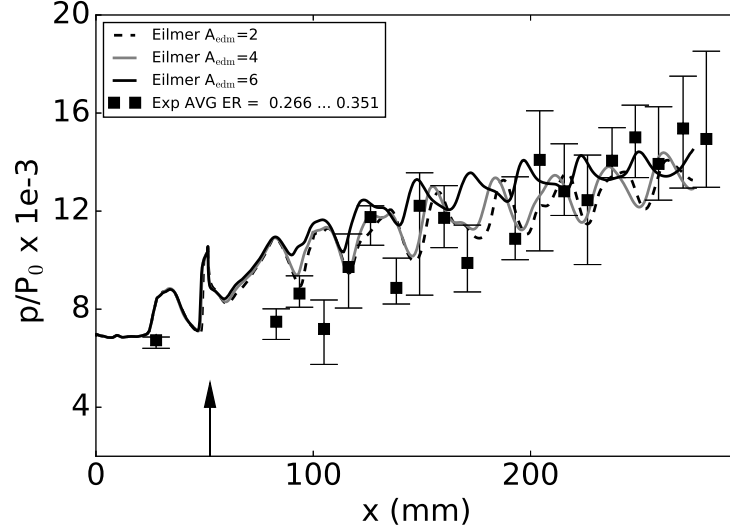

Figure 20: Effect of A_{edm} on the time-averaged pressure traces along the injector wall at y = 9.375 mm and P_0 = 17.73 MPa.

Regarding the use of the EDM for the HyShot II combustor the following conclusions are drawn. Based on the comparison in Table 3, it is inferred that the value of A_{edm} should
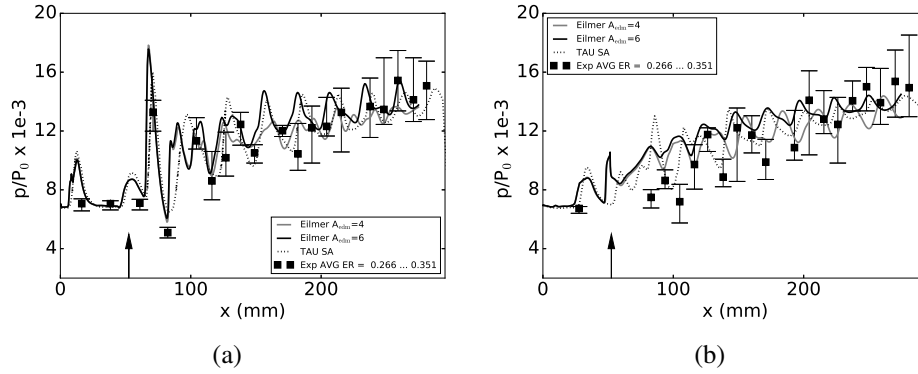
Figure 21: Pressure along the wall at y = 9.375 mm with EDM and no-model reference CFD: (a) cowl side, (b) injector side. P_0 = 17.73 MPa.

be kept below 6. The wall pressure traces in Figures 19 and 20 do confirm this statement. A higher setting would result in even higher peak pressure values which would not agree with experimental measurements until ≈ 200 mm downstream inside the combustor. Further downstream the strength of the combustion is less intense and the CFD predictions are near the lower part of the experimental uncertainty interval, especially on the cowl side. The observation can be explained with the contour of ω in Figure 22. The turbulent dissipation rate is strong inside the barrel shock induced by fuel injection. This is shown in the different cross planes. However, moving downstream, the magnitude reduces considerably (see locations x = 0.15, 0.2 and 0.275 m). As an indication, between locations x = 0.15 and x = 0.07, ω decreases by an order of magnitude (except for the boundary layer). In analogy with the Burrows-Kurkov and DLR configurations, a possibility would be to split the combustor in two zones with a higher A_{edm} value in the downstream region. Overall, a setting A_{edm} between 4 and 6 is advised for the HyShot II combustor.

4.0 DISCUSSION OF THE EDM PREDICTIONS

The experiment of Burrows-Kurkov, the DLR combustor and the HyShot II combustor have been selected in order to investigate the most suitable application of the EDM to supersonic combustion test cases.

In the first test case, the best agreement with several sets of experimental data at the exit of the combustor was achieved with a A_{edm} setting of 6. The value is explained by the configuration with parallel injection of fuel and oxidizer which introduces an ignition delay. In order to capture a similar effect with the EDM, a kinetic limit can be introduced, however the influence is very localized to the near injector region and does not allow to account for a realistic ignition delay. The reaction rate computed with the EDM relies on the value of ω. Its value is high in the shear layer near the injector and decreases downstream of the combustor. In other words, in the region where no combustion takes place experimentally, based on the turbulence, the EDM will predict high reaction rates. In the downstream region the opposite
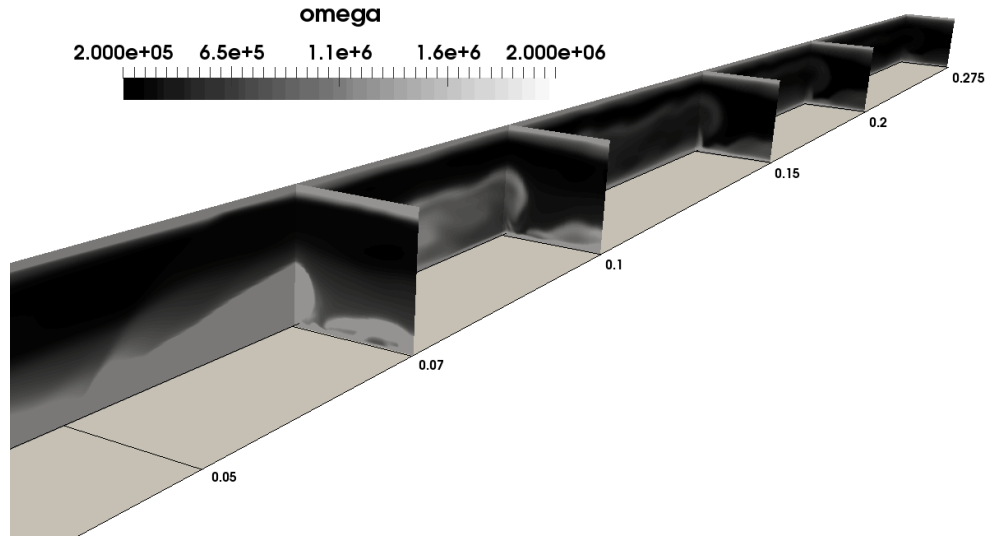
Figure 22: Contour of ω for the HyShot II scramjet combustor.

is true which explains the need for a high A_{edm} value. An alternative to the kinetic limit has been explored in this work and consists of relying on an estimate of the ignition delay from a one-dimensional chemical kinetics program. A comparison with experimental data demonstrated that the approach resulted in improved predictions and could be considered for the analysis of similar scramjet configurations. This was termed a zonal EDM approach.

The DLR test case involves fuel injection behind a strut. Application of the kinetic limited resulted in worse agreement with experimental data in the vicinity of the injector. Varying the EDM constant's value did not strongly affect other quantities aside from the temperature. Just behind the strut, a value between 1 and 4 captures the experimental temperature profile. Further downstream, a value of 4 or higher is more appropriate. These settings are explained by a similar behavior of the turbulence model as in the Burrows-Kurkov test case, i.e. high ω values near the injector with decreasing downstream trend. Based on the DLR combustor results, we suggest a modification of the EDM which consist of a zonal dependency of the A_{edm} value. Close to the point of injection, a lower ($\approx$ 1-4) setting of the A_{edm} constant could be used and further downstream a higher value (> 4). Waidmann et al.[34] discussed the main features inside a configuration such as the DLR combustor. The authors explain the presence of three distinct zones dominated by fundamentally different physics. Firstly there is an induction zone, just behind the strut, where the combustion is dominated by a diffusion process between the injected fuel and vitiated air stream. It is followed by a transitional zone where large scale structures develop. These structures originate in the shear layers between the air and fuel stream due to the velocity difference and vorticity is produced. They are responsible for the entrainment of the oxidizer inside the reaction zone. In this zone, the combustion is dominated by convection instead of diffusion. Further downstream, a third zone is discerned where the turbulent eddies break down and the flow becomes more chaotic. Such information can be used for a better application of the EDM and the idea

of a zonal EDM could apply to the different flow regimes. The extent of the three zones would have to be estimated and the A_{edm} setting adapted. It was shown in the experiment of Burrows and Kurkov that even an estimate of the ignition delay is good enough in order to draw design conclusions with the EDM. The same comment can be made for the DLR combustor. Moreover, the zonal approach could as well be applied to the values of Pr_t and Sc_t.

The HyShot II combustor was selected as a third test case. An A_{edm} setting of 4 provided reasonable predictions of wall pressure traces in comparison with experimental data. Similar to the previous test cases, high values of ω are observed near the point of injection with decreasing value downstream of the combustor. As with the previous test cases, a zonal use of the EDM could be an option to improve agreement with experimental observations. This can also include a variation for the values of Pr_t and Sc_t.

5.0 CONCLUSIONS

In this work the Eddy Dissipation Model (EDM) has been used in conjunction with Wilcox k-ω 2006 turbulence model for the study of three hydrogen-fueled scramjet combustors. A different fuel injection strategy is applied in each of the test cases allowing a broader assessment of the EDM's application. The designs of two of the test cases result in high combustor entrance Mach number (> 2) and static temperature (> 1000 K), typical for high flight Mach numbers (> 8) while one test case was characterized by cold inflow.

The EDM requires the specification of a model constant A_{edm} and the aim of the present work was to understand its most appropriate setting. In the case of parallel fuel injection, a significant ignition delay is present for which the standard application of the EDM, or the EDM with kinetic limit, is unable to account. By relying on an estimate of the ignition delay obtained from a one-dimensional chemical kinetics program, the EDM predictions appear to be in very good agreement with experimental measurements. This indicates that past the point of ignition the combustion appears to be mixing-limited. Without an ignition delay estimate an A_{edm} value of 6 resulted in the best agreement with experimental data while a value of 4 is preferred when an ignition delay is estimated. In the case of hydrogen fuel injection behind a strut, the EDM with kinetic limit failed to predict one of the reaction zones near the strut and was not considered in further simulations. Regarding the setting of the A_{edm} constant, a value of 4 provided overall reasonable results. In the last case of transverse fuel injection, ignition occurs almost as soon as the reactants meet, hence mixing-limited combustion is prevalent. The wall pressure traces obtained with the EDM agreed well with experiments for the largest part of the combustor length. Some differences are observed at the injector wall, especially near the point of injection. An A_{edm} constant value of 4 was identified as appropriate in simulating this combustor. In the discussion of the test cases, a zonal use of the EDM was identified as a viable approach to improve the predictive capability of the model and should be explored in future work. The zonal approach consists of varying the value of A_{edm} across the combustor. It can also be taken further as to vary the setting of Pr_t and Sc_t. With careful calibration of model parameters and the possibility to use a zonal approach, the EDM has the potential to be used in the design of scramjet combustors with hydrogen fuel.

ACKNOWLEDGEMENTS

REFERENCES

1. D Preller and MK Smart. Scramjets for reusable launch of small satellites. In *20th AIAA International Space Planes and Hypersonic Systems and Technologies Conference*, page 3586, 2015.

2. SO Forbes-Spyratos, MP Kearney, MK Smart, and IH Jahn. Trajectory design of a rocket-scramjet-rocket multi-stage launch system. In *21st AIAA International Space Planes and Hypersonics Technologies Conference*, page 2107, 2017.

3. A Ferri. Mixing-controlled supersonic combustion. *Annual Review of Fluid Mechanics*, 5(1):301–338, 1973.

4. A Ingenito and C Bruno. Physics and regimes of supersonic combustion. *AIAA Journal*, 48(3):515, 2010.

5. WO Landsberg, V Wheatley, and A Veeraragavan. Characteristics of cascaded fuel injectors within an accelerating scramjet combustor. *AIAA Journal*, pages 3692–3700, 2016.

6. TF O'Brien, RP Starkey, and MJ Lewis. Quasi-one-dimensional high-speed engine model with finite-rate chemistry. *Journal of propulsion and power*, 17(6):1366–1374, 2001.

7. MK Smart. Scramjets. *The Aeronautical Journal*, 111(1124):605–619, 2007.

8. T Vanyai, M Bricalli, S Brieschenk, and RR Boyce. Scramjet performance for ideal combustion processes. *Aerospace Science and Technology*, 75:215–226, 2018.

9. SM Torrez, JF Driscoll, M Ihme, and ML Fotia. Reduced-order modeling of turbulent reacting flows with application to ramjets and scramjets. *Journal of propulsion and power*, 27(2):371–382, 2011.

10. RA Baurle. Modeling of high speed reacting flows: established practices and future challenges. In *42nd AIAA Aerospace Sciences Meeting and Exhibit*, page 267, 2004.

11. NJ Georgiadis, DA Yoder, MA Vyas, and WA Engblom. Status of turbulence modeling for hypersonic propulsion flowpaths. *Theoretical and Computational Fluid Dynamics*, 28(3):295–318, 2014.

12. BF Magnussen and BH Hjertager. On mathematical modeling of turbulent combustion with special emphasis on soot formation and combustion. In *Symposium (international) on Combustion*, volume 16, pages 719–729. Elsevier, 1977.

13. JR Edwards and JA Fulton. Development of a RANS and LES/RANS flow solver for

high-speed engine flowpath simulations. In *20th AIAA International Space Planes and Hypersonic Systems and Technologies Conference*, page 3570, 2015.

14. TO Mohieldin, SN Tiwari, and David E Reubush. Numerical investigation of dual-mode scramjet combustor with large upstream interaction. 2004.

15. MSR Chandra Murty and D Chakraborty. Numerical simulation of angular injection of hydrogen fuel in scramjet combustor. *Proceedings of the Institution of Mechanical Engineers, Part G: Journal of Aerospace Engineering*, 226(7):861–872, 2012.

16. M Dharavath, P Manna, and D Chakraborty. Thermochemical exploration of hydrogen combustion in generic scramjet combustor. *Aerospace Science and Technology*, 24(1):264–274, 2013.

17. OR Kummitha, KM Pandey, and R Gupta. Cfd analysis of a scramjet combustor with cavity based flame holders. *Acta Astronautica*, 2018.

18. JJOE Hoste. *Scramjet Combustion Modeling Using Eddy Dissipation Model*. PhD thesis, University of Strathclyde, Glasgow, UK, 2018.

19. RJ Gollan and PA Jacobs. About the formulation, verification and validation of the hypersonic flow solver Eilmer. *International Journal for Numerical Methods in Fluids*, 73(1):19–57, 2013.

20. DC Wilcox. Formulation of the k-ω turbulence model revisited. *AIAA Journal*, 46(11):2823–2838, 2008.

21. WYK Chan, PA Jacobs, and DJ Mee. Suitability of the k–ω turbulence model for scramjet flowfield simulations. *International Journal for Numerical Methods in Fluids*, 70(4):493–514, 2012.

22. JJOE Hoste, V Casseau, M Fossati, IJ Taylor, and RJ Gollan. Numerical modeling and simulation of supersonic flows in propulsion systems by open-source solvers. In *21st AIAA International Space Planes and Hypersonics Technologies Conference*, page 2411, 2017.

23. JJOE Hoste, M Fossati, IJ Taylor, and RJ Gollan. Modeling scramjet supersonic combustion via eddy dissipation model. In *68th International Astronautical Congress (IAC), Adelaide*, 2017.

24. MN Macrossan. The equilibrium flux method for the calculation of flows with non-equilibrium chemical reactions. *Journal of Computational Physics*, 80(1):204–231, 1989.

25. MS Liou. Ten years in the making - AUSM-family. *AIAA Paper*, pages 2001–2521, 2001.

26. PA Jacobs, RJ Gollan, AJ Denman, BT O'Flaherty, DF Potter, PJ Petrie-Repar, and IA Johnston. Eilmer's theory book: basic models for gas dynamics and thermochemistry. Technical report, The University of Queensland, 2012.

27. S Gordon and BJ McBride. *Computer program for calculation of complex chemical equilibrium compositions and applications. I.Analysis*. Citeseer, 1996.

28. T Poinsot and D Veynante. *Theoretical and Numerical Combustion, third edition*. RT Edwards, Inc., 2012.

29. J Urzay. Supersonic combustion in air-breathing propulsion systems for hypersonic flight. *Annual Review of Fluid Mechanics*, 50:593–627, 2018.

30. B Sekar and HS Mukunda. A computational study of direct simulation of high speed mixing layers without and with chemical heat release. In *Symposium (International) on Combustion*, volume 23, pages 707–713. Elsevier, 1991.

31. TG Drozda, RA Baurle, and JP Drummond. Impact of flight enthalpy, fuel simulant, and chemical reactions on the mixing characteristics of several injectors at hypervelocity flow conditions. Technical report, NASA Langley Research Center, Hampton, VA, United States, 2016.

32. MC Burrows and AP Kurkov. An analytical and experimental study of supersonic combustion of hydrogen in vitiated air stream. *AIAA Journal*, 11(9):1217–1218, 1973.

33. MC Burrows and AP Kurkov. Analytical and experimental study of supersonic combustion of hydrogen in a vitiated airstream. Technical report, NASA Lewis Research Center, September 1973.

34. W Waidmann, F Alff, U Brummund, M Böhm, W Clauss, and M Oschwald. Experimental investigation of the combustion process in a supersonic combustion ramjet (scramjet). *DGLR Jahrbuch*, pages 629–638, 1994.

35. S Karl, K Hannemann, A Mack, and J Steelant. CFD analysis of the HyShot II scramjet experiments in the HEG shock tunnel. In *15th AIAA International Space Planes and Hypersonic Systems and Technologies Conference*, page 2548, 2008.

36. S Karl. *Numerical investigation of a generic scramjet configuration*. PhD thesis, Saechsische Landesbibliothek-Staats-und Universitaetsbibliothek Dresden, 2011.

37. R Pecnik, VE Terrapon, F Ham, G Iaccarino, and H Pitsch. Reynolds-averaged navier-stokes simulations of the hyshot ii scramjet. *AIAA journal*, 50(8):1717–1732, 2012.

38. J Larsson, S Laurence, I Bermejo-Moreno, J Bodart, S Karl, and R Vicquelin. Incipient thermal choking and stable shock-train formation in the heat-release region of a scramjet combustor. part ii: Large eddy simulations. *Combustion and Flame*, 162(4):907–920, 2015.

39. FR Menter. Two-equation eddy-viscosity turbulence models for engineering applications. *AIAA Journal*, 32(8):1598–1605, 1994.

40. JS Evans and CJ Schexnayder. Influence of chemical kinetics and unmixedness on burning in supersonic hydrogen flames. *AIAA Journal*, 18(2):188–193, 1980.

41. HB Ebrahimi. CFD validation for scramjet combustor and nozzle flows, part I. *AIAA Paper*, page 1840, 1993.

42. B Parent and JP Sislian. Validation of the wilcox k-omega model for flows characteristic to hypersonic airbreathing propulsion. *AIAA Journal*, 42(2):261–270, 2004.

43. WA Engblom, FC Frate, and Nelson CC. Progress in validation of Wind-US for ramjet/scramjet combustion. In *43rd AIAA Aerospace Sciences Meeting and Exhibit*, Reno, Nevada, January 2005.

44. X Xiao, HA Hassan, and RA Baurle. Modeling scramjet flows with variable turbulent Prandtl and Schmidt numbers. *AIAA journal*, 45(6):1415–1423, 2007.

45. P Keistler. *A variable turbulent Prandtl and Schmidt number model study for scramjet applications*. PhD thesis, North Carolina State University, US, 2009.

46. Z Gao, C Jiang, S Pan, and CH Lee. Combustion heat-release effects on supersonic compressible turbulent boundary layers. *AIAA Journal*, 53(7):1949–1968, 2015.

47. JR Edwards, JA Boles, and RA Baurle. Large-eddy/Reynolds-averaged Navier–Stokes simulation of a supersonic reacting wall jet. *Combustion and Flame*, 159(3):1127–1138, 2012.

48. JH Kim, Y Yoon, IS Jeung, H Huh, and J-Y Choi. Numerical study of mixing enhancement by shock waves in model scramjet engine. *AIAA Journal*, 41(6):1074–1080, 2003.

49. V Bhagwandin, W Engblom, and N Georgiadis. Numerical simulation of a hydrogen-fueled dual-mode scramjet engine using Wind-US. In *45th AIAA/ASME/SAE/ASEE Joint Propulsion Conference & Exhibit*, page 5382, 2009.

50. DA Bittker and VJ Scullin. General chemical kinetics computer program for static and flow reactions, with application to combustion and shock-tube kinetics. 1972.

51. RM Kirchhartz, DJ Mee, RJ Stalker, PA Jacobs, and MK Smart. Supersonic boundary-layer combustion: effects of upstream entropy and shear-layer thickness. *Journal of Propulsion and Power*, 26(1):57–66, 2010.

52. M Oevermann. Numerical investigation of turbulent hydrogen combustion in a scramjet using flamelet modeling. *Aerospace science and technology*, 4(7):463–480, 2000.

53. A Mura and JF Izard. Numerical simulation of supersonic nonpremixed turbulent combustion in a scramjet combustor model. *Journal of Propulsion and Power*, 26(4):858–868, 2010.

54. Z Gao, J Wang, C Jiang, and C Lee. Application and theoretical analysis of the flamelet model for supersonic turbulent combustion flows in the scramjet engine. *Combustion Theory and Modelling*, 18(6):652–691, 2014.

55. L Hou, D Niu, and Z Ren. Partially premixed flamelet modeling in a hydrogen-fueled supersonic combustor. *International Journal of Hydrogen Energy*, 39(17):9497–9504, 2014.

56. OR Kummitha. Numerical analysis of hydrogen fuel scramjet combustor with turbulence development inserts and with different turbulence models. *International Journal of Hydrogen Energy*, 42(9):6360–6368, 2017.

57. F Génin and S Menon. Simulation of turbulent mixing behind a strut injector in supersonic flow. *AIAA Journal*, 48(3):526, 2010.

58. AS Potturi and JR Edwards. Hybrid Large-Eddy/Reynolds-averaged Navier–Stokes simulations of flow through a model scramjet. *AIAA Journal*, 2014.

59. C Fureby, E Fedina, and J Tegnér. A computational study of supersonic combustion behind a wedge-shaped flameholder. *Shock waves*, 24(1):41–50, 2014.

60. ED Gonzalez-Juez, AR Kerstein, R Ranjan, and S Menon. Advances and challenges in modeling high-speed turbulent combustion in propulsion systems. *Progress in Energy and Combustion Science*, 60:26–67, 2017.

61. RH Nichols and CC Nelson. Wall function boundary conditions including heat transfer and compressibility. *AIAA journal*, 42(6):1107–1114, 2004.

62. S Karl, S Laurence, JM Schramm, and K Hannemann. CFD Analysis of Unsteady Combustion Phenomena in the HyShot-II Scramjet Configuration. In *18th AIAA/3AF International Space Planes and Hypersonic Systems and Technologies Conference*, page 5912, 2012.

63. TJ Barth and H Deconinck. *High-order methods for computational physics*, volume 9. Springer Science & Business Media, 2013.